


ORIGINAL RESEARCH

# Angiotensin Receptor-Neprilysin Inhibition Attenuates Right Ventricular Remodeling in Pulmonary Hypertension

Danial Sharifi Kia, MSc; Evan Benza, BSc; Timothy N. Bachman, MSc; Claire Tushak; Kang Kim, PhD; Marc A. Simon , MD, MSc

**BACKGROUND:** Pulmonary hypertension (PH) results in increased right ventricular (RV) afterload and ventricular remodeling. Sacubitril/valsartan (sac/val) is a dual acting drug, composed of the neprilysin inhibitor sacubitril and the angiotensin receptor blocker valsartan, that has shown promising outcomes in reducing the risk of death and hospitalization for chronic systolic left ventricular heart failure. In this study, we aimed to examine if angiotensin receptor-neprilysin inhibition using sac/val attenuates RV remodeling in PH.

**METHODS AND RESULTS:** RV pressure overload was induced in Sprague–Dawley rats via banding the main pulmonary artery. Three different cohorts of controls, placebo-treated PH, and sac/val-treated PH were studied in a 21-day treatment window. Terminal invasive hemodynamic measurements, quantitative histological analysis, biaxial mechanical testing, and constitutive modeling were employed to conduct a multiscale analysis on the effects of sac/val on RV remodeling in PH. Sac/val treatment decreased RV maximum pressures (29% improvement,  $P=0.002$ ), improved RV contractile (30%,  $P=0.012$ ) and relaxation (29%,  $P=0.043$ ) functions, reduced RV afterload (35% improvement,  $P=0.016$ ), and prevented RV-pulmonary artery uncoupling. Furthermore, sac/val attenuated RV hypertrophy (16% improvement,  $P=0.006$ ) and prevented transmural reorientation of RV collagen and myofibers ( $P=0.011$ ). The combined natriuresis and vasodilation resulting from sac/val led to improved RV biomechanical properties and prevented increased myofiber stiffness in PH (61% improvement,  $P=0.032$ ).

**CONCLUSIONS:** Sac/val may prevent maladaptive RV remodeling in a pressure overload model via amelioration of RV pressure rise, hypertrophy, collagen, and myofiber reorientation as well as tissue stiffening both at the tissue and myofiber level.

**Key Words:** biomechanics ■ hemodynamics ■ pulmonary hypertension ■ right ventricular remodeling ■ sacubitril/valsartan

## See Editorial by Verbrugge and Borlaug

**P**ulmonary hypertension (PH) is a disease resulting in increased right ventricular (RV) afterload, myocardial hypertrophy, and ventricular remodeling. RV failure remains the main cause of mortality for nearly 70% of PH patients<sup>1</sup> with 33% to 38% mortality rates 3 years post diagnosis.<sup>2,3</sup> Pressure overload due to PH results in increased end-systolic and end-diastolic volumes as well as increased RV contractility,<sup>4</sup> which,

if left unchecked, leads to decreased RV contractility and eventual RV failure. Despite the development of multiple therapeutics for management of PH, lung transplantation remains the only curative treatment.

RV biomechanics has been closely linked to RV function.<sup>5</sup> From a biomechanical point of view, pressure overloaded RV myocardium experiences increased wall thickness, fiber remodeling, and increased stiffness to

Correspondence to: Marc A. Simon, MD, MSc, Division of Cardiology, Department of Medicine, University of Pittsburgh School of Medicine, Presbyterian University Hospital C-701, 200 Lothrop St, Pittsburgh, PA. E-mail: simonma@upmc.edu

Supplementary Materials for this article are available at <https://www.ahajournals.org/doi/suppl/10.1161/JAHA.119.015708>

This article was handled independently by John Jefferies, MD as a guest editor. The editors had no role in the evaluation of the manuscript or in the decision about its acceptance.

For Sources of Funding and Disclosures, see page 12.

© 2020 The Authors. Published on behalf of the American Heart Association, Inc., by Wiley. This is an open access article under the terms of the Creative Commons Attribution-NonCommercial License, which permits use, distribution and reproduction in any medium, provided the original work is properly cited and is not used for commercial purposes.

JAHA is available at: [www.ahajournals.org/journal/jaha](http://www.ahajournals.org/journal/jaha)

## CLINICAL PERSPECTIVE

### What Is New?

- Sacubitril/valsartan was studied in an animal model of pulmonary hypertension and prevented myocyte remodeling, stiffening, and fiber angle reorientation.
- This study provides a potential insight into the right ventricular remodeling process in pulmonary hypertension in which progressive pressure overload and increasing wall stress result in alterations of the myocyte contractile apparatus.
- This, in turn, may lead to progressive myofiber stiffening and fiber angle reorientation and ultimately to right ventricular failure.

### What Are the Clinical Implications?

- Sacubitril/valsartan and targeting the myocyte contractile apparatus may be a promising therapy for pulmonary hypertension to prevent right ventricular remodeling and failure.

## Nonstandard Abbreviations and Acronyms

<b>dp/dt max, min</b>	maximum and minimum of the time derivative of pressure (load-dependent measures of contractility and relaxation)
<b>Ea</b>	PA elastance (measure of afterload)
<b>Ees</b>	RV elastance (load-independent measure of contractility)
<b>Ees/Ea</b>	measure of RV-PA coupling
<b>LV</b>	left ventricle
<b>PA</b>	pulmonary artery
<b>PH</b>	pulmonary hypertension
<b>RV</b>	right ventricle
<b>RVFW</b>	right ventricular free wall
<b>sac/val</b>	sacubitril/valsartan

restore cardiac output. RV remodeling and fiber reorientation results in a pathological increase in stiffness and nonphysiologic anisotropy in certain directions, which affects the filling and ejection mechanics of the RV,<sup>6</sup> torsional motion of the heart, and transmural wall stress.<sup>7</sup> Biomechanical studies have provided important insights into RV remodeling in response to PH<sup>4–6,8,9</sup>; however, limited information exists on the effects of therapeutic interventions on these mechanisms.<sup>10</sup>

Sacubitril/valsartan (sac/val; also known as LCZ696) is an angiotensin receptor-neprilysin inhibitor drug

consisting of a 1:1 mixture of the neprilysin inhibitor sacubitril and the angiotensin receptor blocker valsartan, which is approved by the Food and Drug Administration to reduce the risk of cardiovascular death and heart failure hospitalization for chronic systolic left ventricular (LV) heart failure.<sup>11</sup> Despite promising outcomes as a treatment for chronic systolic LV heart failure<sup>12</sup> and demonstrating antifibrotic and anti-inflammatory effects,<sup>13–16</sup> to date, there are limited data on the effects of sac/val treatment on RV remodeling in PH.

In the current study, we aimed to understand the response of RV myocardium in PH to treatment with sac/val. We hypothesized that preventive treatment of PH with sac/val attenuates the development of RV hypertrophy and results in improved RV biomechanics. Terminal invasive hemodynamic measurements, quantitative histological analysis, biaxial mechanical testing, and constitutive modeling were employed to conduct a multiscale analysis on the effects of sac/val on RV remodeling.

## METHODS

The data that support the findings of this study are available from the corresponding author upon reasonable request. A rat model of PH (total of 58 male Sprague–Dawley rats) was used to evaluate the effects of sac/val treatment on the biomechanical properties of failing RV myocardium. Hemodynamic measurements were performed at the end of the treatment window, followed by biaxial mechanical testing of the right ventricular free wall (RVFW). An additional group of animals were used for quantitative histological analysis of RV collagen and myofiber architecture. Figure 1 summarizes the cohorts, experimental protocols, and different analysis techniques used in this work. All animal procedures were approved by the University of Pittsburgh's institutional animal care and use committee (protocol # 13021226) and were carried out in such a way as to minimize discomfort, distress, pain, and injury to animals. All surgical procedures were performed under isoflurane anesthesia followed by bupivacaine (2–3 mg/kg), buprenorphine (0.05–0.1 mg/kg), and ketoprofen (1 mg/kg) administered as pain medications during and post surgery. The animals were euthanized by harvesting the heart following hemodynamic data collection.

### Pulmonary Artery Banding Procedures and Drug Administration

RV pressure overload was induced via banding the main pulmonary artery (PA) of male Sprague–Dawley rats using an adjustable surgical clip (n=40, ≈8 weeks old, weighing 200–250 g at the start of the experiments, sourced from Envigo, Indianapolis, IN).

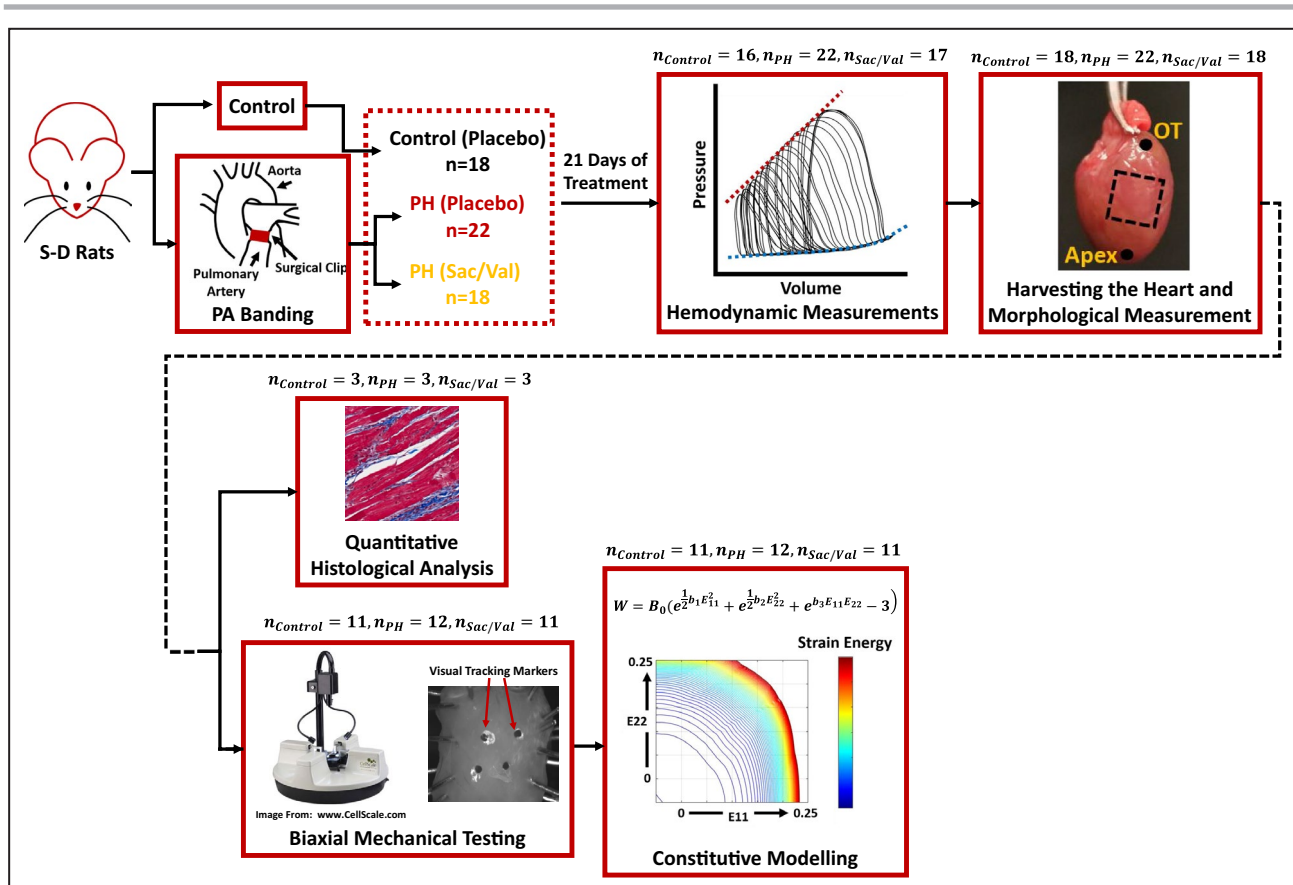


**Figure 1. Summary of the framework developed to study the effects of sac/val on RV remodeling in PH.**

Sprague–Dawley rats were assigned to one of the control, PH-placebo treated, or PH-sac/val treated cohorts, followed by terminal invasive hemodynamic measurements, morphological measurements, quantitative histological analysis, biaxial mechanical characterization, and constitutive modeling. OT indicates outflow tract; PA banding, pulmonary artery banding; PH, pulmonary hypertension; RV, right ventricle; Sac/Val, sacubitril/valsartan; and S-D Rats, Sprague–Dawley Rats.

To the best of our knowledge, no sex-based differences have been reported for RV biomechanics in the literature and, therefore, we chose to study only male rats in the current work. This would be an important topic for future research. As discussed in our previous studies,<sup>4,17</sup> several factors were considered for our choice of this animal model. Briefly, this model causes RV pressure overload in the absence of confounding conditions, such as hypoxia, sufficient to study RV remodeling; a rat model was selected to provide a large enough sample of RVFW tissue for biaxial mechanical testing, while being thin enough to facilitate biaxial mechanical testing of intact full-thickness myocardium without the need for transmural sectioning as well as maintaining tissue viability *ex vivo* via passive diffusion.

Once anesthetized, rats were placed on a heated table to maintain a core temperature of 37°C and were monitored with a rectal probe. After endotracheal intubation, animals were placed on a volume ventilator (70 breaths/min, 6–8 mL/kg per minute). The chest was then entered by a limited lateral incision to expose

the midthoracic aorta. The PA was identified, and a surgical clip was placed around it with a radius such that a uniform RV systolic pressure of 40 to 50 mm Hg was generated acutely (confirmed via hemodynamic measurements in pilot studies). The chest was then closed, and animals were extubated. Following the pulmonary artery banding procedure, rats were randomized into 2 cohorts: placebo-treated PH and sac/val-treated PH (Figure 1). Additionally, a control group (n=18) consisted of unbanded age-matched placebo-treated animals. Daily doses of sac/val (68 mg/kg per day) or placebo (same volume of water) were administered via oral gavage for 21 days.<sup>14,15</sup>

### Hemodynamic Measurements

Following the treatment window, terminal invasive hemodynamic measurements were performed to confirm RV pressure overload via standard catheterization techniques.<sup>4,18,19</sup> RV pressure-volume loops were acquired for each animal ( $n_{\text{Control}} = 16, n_{\text{PH}} = 22, n_{\text{sac/val}} = 17$ ), using a Millar™ conductance catheter (Millar Inc., Houston, TX).

Hemodynamic data were processed using LabChart (ADInstruments, Sydney, Australia) and analyzed for measures of cardiac function, including maximum pressure, stroke volume, heart rate, maximum and minimum  $\frac{dp}{dt}$ , RV elastance (Ees), PA elastance (Ea), and RV-PA coupling (Ees/Ea). RV maximum pressure was measured as the difference between maximum and minimum pressures of a beat. RV elastance was measured via occlusion of the vena cava.<sup>4</sup> Due to volume measurements performed in relative volume units, only relative volumetric data (such as stroke volume and Ees) are reported and used for data analysis. The heart was then harvested and placed in cardioplegic solution.

### Histological Analysis

A subgroup of rats from each cohort were used for histological analysis. On the basis of our previous studies using this model of PH,<sup>4</sup> a sample size of  $n=3/\text{cohort}$  was chosen for this aim with the primary goal of studying transmural RV fiber orientations. Specimen fixation was performed using 10% neutral buffered formalin. Histology was carried out using Masson's trichrome, which distinctly stains myofibers in red and collagen in blue. A total of 21 to 25 transmural sections were taken from each RVFW specimen at 50  $\mu\text{m}$  increments from epicardium to endocardium. Collagen (blue) and myofibers (red) were segmented from the histological scans by manual thresholding of images based on the appropriate RGB range. Area fraction of collagen fibers (measure of fibrosis) was evaluated by calculating the ratio of area occupied by the respective pixels (blue) over the total area in each cross-section. Average of all transmural measurements are reported as the collagen area fraction for each RVFW specimen. Transmural fiber orientation of collagen and myofibers were quantitatively analyzed using a gradient-based image analysis framework. Similar to our previous studies,<sup>4</sup> the orientation angle and magnitude of the gradient were calculated at each pixel, followed by the formation of the structure tensor of the gradient map for each histological section:

$$H = \begin{bmatrix} \sum_{i,j=1}^{i=n,j=m} G_{i,j}^2 \cos^2 \Phi_{i,j} & \sum_{i,j=1}^{i=n,j=m} G_{i,j}^2 \cos \Phi_{i,j} \sin \Phi_{i,j} \\ \sum_{i,j=1}^{i=n,j=m} G_{i,j}^2 \cos \Phi_{i,j} \sin \Phi_{i,j} & \sum_{i,j=1}^{i=n,j=m} G_{i,j}^2 \sin^2 \Phi_{i,j} \end{bmatrix} \quad (1)$$

Here,  $G_{i,j}$  and  $\Phi_{i,j}$  are the magnitude of the gradient and the orientation angle at each point, respectively. Dominant fiber orientations at each section were obtained by evaluating the dominant orientation (first eigenvector) of the resulting structure tensor from each

histological image.<sup>20,21</sup> Transmural fiber angles are reported against normalized RVFW thickness at 11 different cross-sections (0–100% thickness). Linear interpolations were performed to report the final data for all cohorts on an evenly spaced grid. On the basis of our previous studies on this model of PH,<sup>4</sup> linear interpolations adequately approximate the transmural change in fiber angles. We assigned 0° to the longitudinal (apex to outflow tract) and 90° to the circumferential (free wall to septum) direction, when looking at the RVFW from the epicardium.

In addition to fiber orientations, coherency of collagen fiber distributions was calculated to analyze the structural arrangement of collagen fibers in each layer:

$$C = \frac{\lambda_{\max} - \lambda_{\min}}{\lambda_{\max} + \lambda_{\min}} \times 100 \quad (2)$$

Here,  $\lambda_{\max}$  and  $\lambda_{\min}$  are the first and second eigenvectors of the structure tensor in Equation 1, respectively.<sup>20</sup> Coherency evaluates the local alignment of collagen fibers with  $C=0\%$  indicating an isotropic distribution and  $C=100\%$  indicating a highly aligned pattern. This helps evaluating the level of collagen crimp in each cohort (higher C indicating less crimp), as an important contributor to tissue architecture and biomechanical properties. Average of all transmural measurements are reported as %collagen coherency for each specimen. Furthermore, RVFW area was obtained for each specimen based on histological sections followed by calculation of RVFW wet tissue density by dividing RVFW mass by volume (area $\times$ wall thickness). Image processing and fiber orientation analysis were performed using the OrientationJ toolbox<sup>20,21</sup> in ImageJ (imagej.nih.gov).

### Biaxial Mechanical Testing

Another group of rats from each cohort ( $n_{\text{Control}}=11, n_{\text{PH}}=12, n_{\text{Sac/Val}}=11$ ) underwent biaxial mechanical testing to investigate the effects of sac/val treatment on the biomechanical properties of viable RV myocardium in PH. Square specimens were dissected from the RVFW and mounted on a biaxial testing device (BioTester, CellScale, Waterloo, ON, Canada) using sutures and metal hooks to minimize shear loading.<sup>22</sup> The RVFW was submerged in modified Krebs's solution with 2,3-butanedione monoxime (BDM) and oxygen<sup>17</sup> during testing. Our previous studies have shown the effectiveness of this technique in maintaining tissue viability via passive diffusion, up to 1.5 hours post harvesting.<sup>4</sup> Multiprotocol biaxial testing was performed on each specimen to investigate the tissue response in a wide range of possible loading scenarios (displacement-controlled 1:1, 1:2, 1:4, and 1:6 loading ratios). A set of 4 visual



tracking markers were placed on the epicardium. Marker displacements were recorded using a CCD camera and further analyzed for strain estimations. The deformation gradient tensor was then reconstructed from recorded marker displacements as<sup>23</sup>:

$$F = \frac{dx}{dX} \quad (3)$$

where  $F$  is the deformation gradient tensor,  $X$  is the reference coordinate, and  $x$  is the deformed coordinate system. Using  $F$ , components of the Green–Lagrange strain tensor ( $E$ ) were calculated as:

$$E = \frac{1}{2}(F^T F - I) \quad (4)$$

Load measurements from the biaxial device and initial specimen dimensions were used to reconstruct the first Piola–Kirchhoff stress tensor ( $P$ ) via standard methods.<sup>4,17</sup> The second Piola–Kirchhoff stress tensor ( $S$ ) was then calculated as:

$$S = P F^{-T} \quad (5)$$

A plane stress approximation was used to calculate the biomechanical behavior of RVFW. Stress-strain response of each specimen was calculated using a finite deformation framework developed in Mathcad (PTC, Needham, MA). Equibiaxial stress-strain response of tissues were interpolated from the multiprotocol experimental data using previously established techniques.<sup>4,24</sup> Similar to prior studies,<sup>4,24</sup> fiber-level properties were obtained from the equibiaxial data, which represent the combined myofiber and collagen stress-strain response of the RVFW independent of fiber orientation and mitigate any possible sample mounting/misalignment errors during experimental testing. Fiber-level properties were used for direct estimation of the intrinsic myofiber stiffness for specimens in each cohort. Myofibers were assumed to be mainly responsible for the initial portion of the stress-strain curve, followed by collagen recruitment (un-crimping) and a stiffer high-stress response. The fiber-level stress response for each specimen was differentiated with respect to strain in order to evaluate tissue stiffness changes over the range of measured strain. The general behavior observed for specimens included a relatively constant-stiffness region (myofibers) followed by an increased tissue stiffness region (collagen recruitment). The fiber-level stress-strain data before the start of collagen recruitment was used for estimating myofiber properties for each specimen using a rule of mixtures approach<sup>25</sup>:

$$E_{Myofiber} = \frac{TM_{Before\ Collagen\ Recruitment}}{\Phi_{Myofiber}} \quad (6)$$

Here,  $E_{Myofiber}$  is the intrinsic myofiber stiffness,  $TM_{Before\ Collagen\ Recruitment}$  is the slope of the line fitted to the fiber-level stress-strain data before collagen recruitment strain (via linear regression) and  $\Phi_{Myofiber}$  is the area fraction of myofibers in each cohort obtained from histological analysis.

## Constitutive Modeling

The experimentally obtained stress-strain data were used to model the response of specimens using a nonlinear anisotropic constitutive model<sup>26</sup>:

$$W = B_0(e^{\frac{1}{2}b_1 E_{11}^2} + e^{\frac{1}{2}b_2 E_{22}^2} + e^{b_3 E_{11} E_{22}} - 3) \quad (7)$$

Here,  $W$  is the strain energy,  $B_0$  is a scaling factor,  $b_1$  is a metric for stiffness in the longitudinal direction (apex to outflow tract direction),  $b_2$  is a metric for stiffness in the circumferential direction,  $b_3$  represents the degree of longitudinal-circumferential coupling, and  $E_{11}$  and  $E_{22}$  are the longitudinal and circumferential Green–Lagrange strains, respectively. By differentiating the strain energy function ( $W$ ) with respect to strain, stress components were obtained as:

$$\begin{aligned} S_{11} &= \frac{\partial W}{\partial E_{11}} = B_0(b_1 E_{11} e^{\frac{1}{2}b_1 E_{11}^2} + b_3 E_{22} e^{b_3 E_{11} E_{22}}) \\ S_{22} &= \frac{\partial W}{\partial E_{22}} = B_0(b_2 E_{22} e^{\frac{1}{2}b_2 E_{22}^2} + b_3 E_{11} e^{b_3 E_{11} E_{22}}) \end{aligned} \quad (8)$$

Here,  $S_{11}$  and  $S_{22}$  are the second Piola–Kirchhoff stress components in the longitudinal and circumferential directions, respectively. Experimental stress-strain data were used to estimate model parameters for each specimen based on Equation 8. Parameter estimation was performed using a custom nonlinear least-squares optimization algorithm (trust-region-reflective) in MATLAB (Mathworks, Natick, MA). Goodness of fit was evaluated using a  $R^2$  measure. Model parameters were compared to analyze the effects of PH and sac/val treatment on RVFW anisotropy and stiffness in different directions ( $B_0 \times b_1$ ,  $B_0 \times b_2$  and  $B_0 \times b_3$  reported as “Longitudinal Stiffness,” “Circumferential Stiffness,” and “Coupled Stiffness” respectively<sup>27</sup>). Biomechanical responses were compared by investigating the model-derived strain energy space for specimens in each cohort. Cohort-specific strain energy maps (in the longitudinal-circumferential strain space) were generated using the median of all strain energy distributions for specimens in each cohort.

## Statistical Analysis

Transmural distribution of collagen and myofiber angles, collagen area fraction and coherency, biaxial

mechanical properties, and fiber-level stress-strain data are reported as mean $\pm$ SD. All other data are presented with median, mean, SD, and interquartile range.

Sample normality and homoscedasticity were assessed using the Shapiro–Wilk test and Bartlett’s test, respectively, in order to identify the appropriate parametric/nonparametric test for our analysis. For the transmural fiber orientation measurements, circular statistics were used to calculate the circular mean and SD, followed by statistical testing using the Watson–Williams test (equivalent of 1-way ANOVA for circular data). Comparisons were performed using the CircStat toolbox<sup>28</sup> in MATLAB. All other histological data (n=3) were analyzed by 1-way ANOVA followed by post hoc *t* tests with Bonferroni correction. For all other data, statistical analysis was performed using the Kruskal–Wallis test. In case of statistical significance, pairwise Wilcoxon rank sum tests were performed for post hoc

testing with Bonferroni correction. Statistical comparisons were performed using the R software package<sup>29</sup> (R Foundation for Statistical Computing, Vienna, Austria, www.R-project.org). For all purposes,  $P < 0.05$  was considered statistically significant.

## RESULTS

### Hemodynamics and Remodeling

Effects of pressure overload and sac/val treatment on RV hemodynamics are demonstrated in Figure 2 ( $n_{\text{Control}} = 16, n_{\text{PH}} = 22, n_{\text{Sac/Val}} = 17$ ). PA banding resulted in significant increase in the maximal RV pressure (Figure 2A;  $67.5 \pm 16.2$  mm Hg for PH versus  $23.8 \pm 2.8$  mm Hg for control). Sac/val treatment demonstrated lower pressures compared with the PH group, while still being higher than control levels

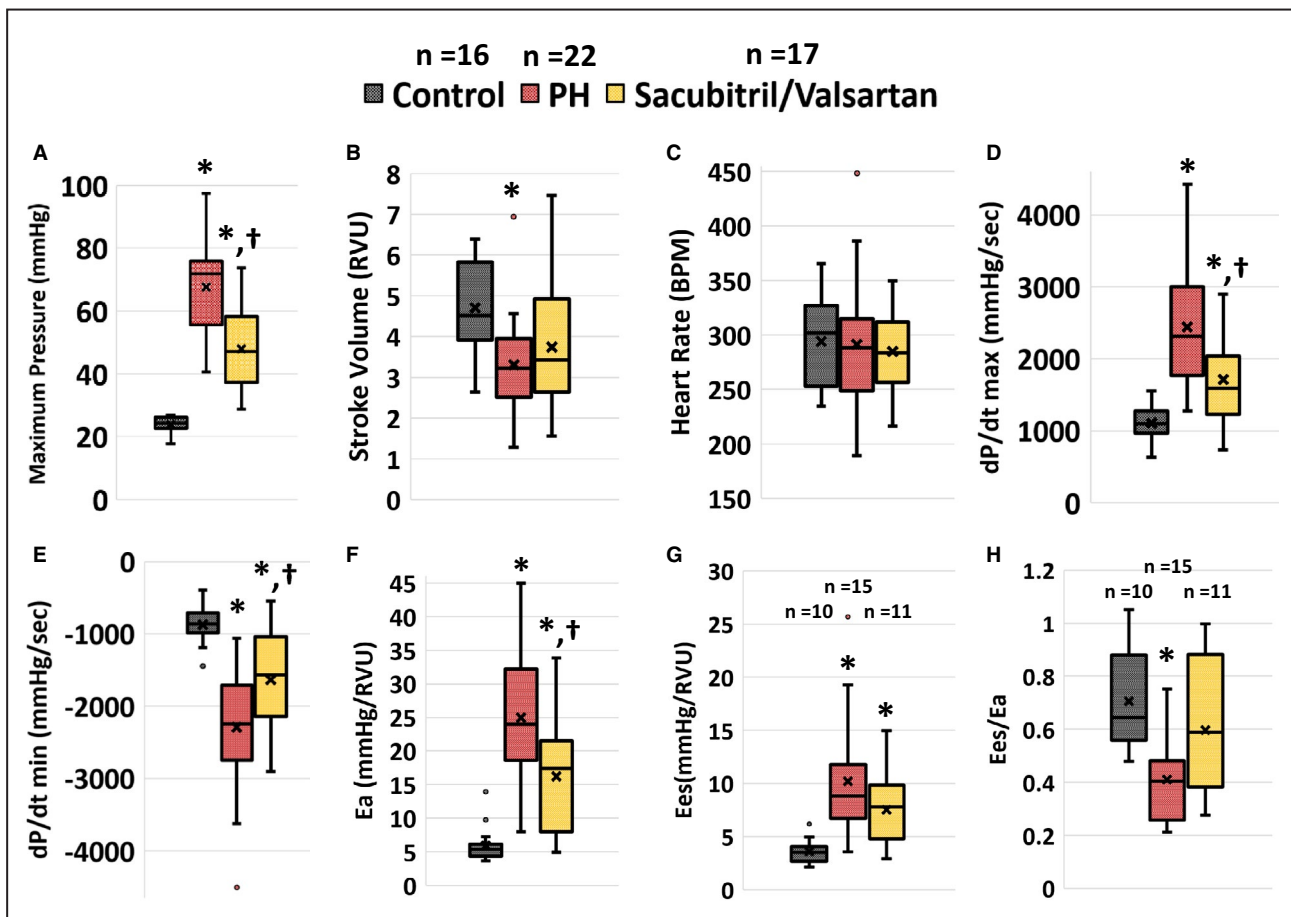


**Figure 2.** Hemodynamic measurements of the effects of PH and sac/val treatment on (A) RV maximum pressure, (B) stroke volume, (C) heart rate, (D)  $dp/dt$  max, (E)  $dp/dt$  min, (F) PA elastance (Ea), (G) RV elastance (Ees), and (H) ratio of RV to PA elastance ( $\frac{Ees}{Ea}$ ).

Sac/val treatment significantly lowered RV maximum pressure ( $P_{\text{max}}$ ), decreased the load-dependent measure of contractility ( $dp/dt$  max), increased the load-dependent measure of relaxation ( $dp/dt$  min) and decreased PA elastance (Ea) in addition to preventing RV-PA uncoupling. Horizontal line (—) and cross (X) representing median and mean of distributions, respectively. Kruskal–Wallis tests with pairwise Wilcoxon rank sum post hoc testing. \* $P < 0.05$  compared with control, † $P < 0.05$  compared with PH.  $\frac{dp}{dt}$  max and min indicates maximum and minimum of the time derivative of pressure; BPM, beats per minute; PA, pulmonary artery; PH, pulmonary hypertension; RV, right ventricle; RVU, relative volume units; and Sac/Val, sacubitril/valsartan.

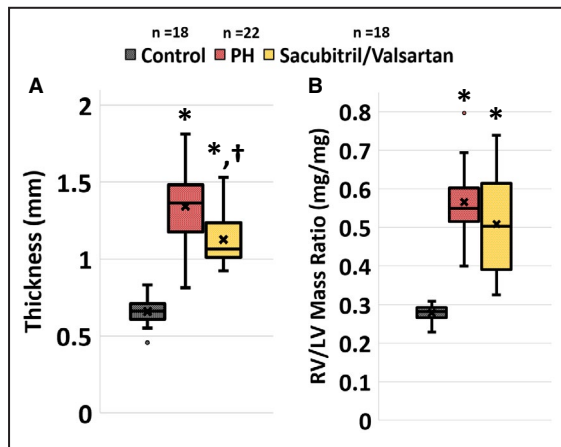


**Figure 3.** Effects of PH and sac/val treatment on (A) RV hypertrophy (RVFW thickness) and (B) RV to LV mass ratio. Sac/val resulted in significantly lower RV wall thickness, while not demonstrating significant effects on RV to LV mass ratio. Horizontal line (—) and cross (X) representing median and mean of distributions, respectively. Kruskal–Wallis tests with pairwise Wilcoxon rank sum post hoc testing. \* $P < 0.05$  compared with control, † $P < 0.05$  compared with PH. LV indicates left ventricle; PH, pulmonary hypertension; RV, right ventricle; RVFW, right ventricular free wall; and Sac/Val, sacubitril/valsartan.

( $47.9 \pm 13.9$  mm Hg). RV stroke volume significantly decreased in response to PH, with sac/val treatment showing no significant effects compared with both control and PH cohorts (Figure 2B;  $4.7 \pm 1.1$ ,  $3.3 \pm 1.2$  and  $3.7 \pm 1.6$  relative volume units for control, PH, and sac/val, respectively). Heart rate was not different among different cohorts (Figure 2C;  $294.0 \pm 39.0$ ,  $291.4 \pm 59.7$  and  $284.9 \pm 37.2$  beats per minute for control, PH, and sac/val, respectively). Maximal and minimal dp/dt (load-dependent measures of RV contractility and relaxation) increased and decreased, respectively, in response to PH (Figure 2D and 2E; dp/dt<sub>max</sub>:  $2440.9 \pm 812.9$  mm Hg/s for PH versus  $1112.2 \pm 242.9$  mm Hg/s for control; dp/dt<sub>min</sub>:  $-2290.1 \pm 844.7$  mm Hg/s for PH versus  $-873.0 \pm 263.2$  mm Hg/s for control). Sac/val treatment significantly decreased dp/dt<sub>max</sub> ( $1719.1 \pm 590.9$  mm Hg/s) and increased dp/dt<sub>min</sub> ( $-1635.2 \pm 684.1$  mm Hg/s) compared with PH levels. Ea (measure of vascular load) increased in PH, and sac/val resulted in significant improvements (Figure 2F;  $5.9 \pm 2.6$ ,  $25.0 \pm 9.1$ , and  $16.2 \pm 8.2$  for control, PH, and sac/val, respectively). Ees (load-independent measure of RV contractility) was obtained only for a subgroup of animals in each cohort ( $n_{\text{Control}} = 10, n_{\text{PH}} = 15, n_{\text{Sac/Val}} = 11$ ) because of difficulties associated with vena cava occlusions. Ees significantly increased in PH and was not affected by sac/val treatment (Figure 2G;  $3.6 \pm 1.2$ ,  $10.2 \pm 5.8$ , and  $7.5 \pm 3.4$  mm Hg/relative volume units for control, PH, and sac/val, respectively). Ratio of Ees to Ea

significantly decreased in PH, indicating decompensated RV-PA coupling. Sac/val treatment prevented a significant drop from control levels (Figure 2H;  $0.71 \pm 0.18$ ,  $0.41 \pm 0.15$ , and  $0.60 \pm 0.24$  for control, PH, and sac/val, respectively). Full statistical results of the hemodynamics are presented in Table S1.

As shown in Figure 3 and Table S2, PH resulted in RVFW hypertrophy (increased wall thickness) and increased RV/LV mass ratio (RVFW thickness:  $1.34 \pm 0.23$  mm for PH versus  $0.66 \pm 0.09$  mm for control; RV/LV mass ratio:  $0.57 \pm 0.08$  for PH versus  $0.28 \pm 0.02$  for control). Sac/val treatment resulted in significant improvements in RVFW hypertrophy ( $1.13 \pm 0.17$  mm), while showing no statistical significance on RV/LV mass ratio ( $0.51 \pm 0.13$ ).

### Fiber Angle

Histological analysis ( $n_{\text{Control}} = 3, n_{\text{PH}} = 3, n_{\text{Sac/Val}} = 3$ ) showed transmural reorientation of collagen and myofibers toward the longitudinal direction (apex to outflow tract) in PH, in addition to increased collagen content and fibrosis (Figure 4A through 4E, Table S3). Collagen fiber orientations were similar to myofiber orientations in each cohort (Figure 4B and 4C). Sac/val treatment prevented transmural reorientation of both collagen and myofibers except for the subendocardial region where fiber reorientation was observed (myofiber angle range from epicardium to endocardium:  $-52.4^\circ \rightarrow +7.4^\circ$ ,  $-56.9^\circ \rightarrow +39.5^\circ$ , and  $-57.8^\circ \rightarrow +25.2^\circ$  for Control, PH, and sac/val, respectively; collagen fiber angle range from epicardium to endocardium:  $-49.9^\circ \rightarrow +2.6^\circ$ ,  $-59.6^\circ \rightarrow +39.0^\circ$ , and  $-66.0^\circ \rightarrow +24.0^\circ$  for control, PH, and sac/val, respectively). Dominant transmural orientation of collagen and myofibers for specimens in each cohort was obtained by calculating the circular mean of the transmural distribution of fiber angles (dotted lines in Figure 4B and 4C). As shown in Figure 4D, PH resulted in rotation of the dominant orientation of myofibers toward the longitudinal direction by  $\approx 15.5^\circ$ , whereas sac/val prevented this remodeling (dominant transmural myofiber orientation:  $-21.1 \pm 0.1^\circ$ ,  $-5.8 \pm 3.2^\circ$ , and  $-19.8 \pm 3.0^\circ$  for control, PH, and sac/val, respectively). Collagen area fraction (measure of fibrosis) increased in response to PH whereas sac/val treatment did not result in significant improvements (Figure 4E; collagen area fraction:  $5.5 \pm 1.1\%$ ,  $12.4 \pm 2.7\%$ , and  $10.8 \pm 0.8\%$  for control, PH, and sac/val, respectively). Collagen fiber coherency (Figure 4F) did not show any statistically significant differences for either PH or sac/val cohorts ( $16.5 \pm 1.5\%$ ,  $21.1 \pm 2.5\%$ , and  $21.1 \pm 2.1\%$  for control, PH, and sac/val, respectively). Furthermore, RVFW area showed no statistically significant differences in either cohort ( $67.2 \pm 2.0$ ,  $105.4 \pm 14.5$ , and  $85.5 \pm 23.3$  mm<sup>2</sup> for control, PH, and sac/val, respectively). Bulk RVFW wet tissue density significantly decreased in PH that was

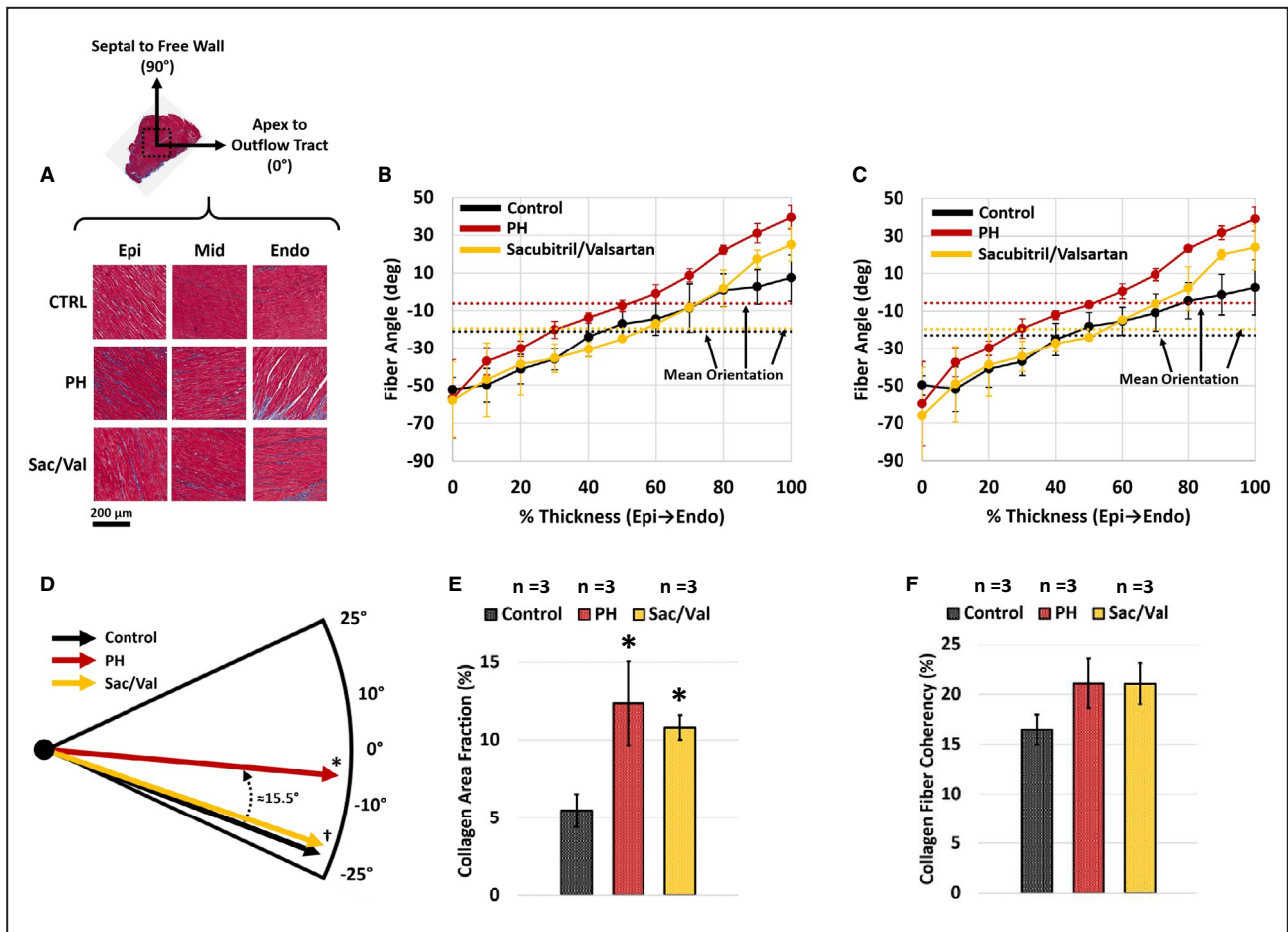


**Figure 4. Histological analysis of the effects of sac/val treatment on RV remodeling in PH.**

**A**, Representative transverse histological sections of RV myocardium from each cohort (Red: Myofiber, Blue: Collagen). Coordinates used to measure fiber orientations indicated on the top. Dashed square representing the specimen orientation used for biaxial testing. **B**, Effects of sac/val treatment on transmural myofiber orientations. **C**, Effects of sac/val treatment on transmural collagen fiber orientations. **D**, Dominant myofiber orientation in each cohort (Watson–Williams test). **E**, Effects of sac/val on RV collagen area fraction (1-way ANOVA followed by post hoc *t* tests). **F**, Effects of sac/val on RV collagen fiber coherency (1-way ANOVA followed by post hoc *t* tests). Error bars representing SD. \**P*<0.05 compared with control, †*P*<0.05 compared with PH. CTRL indicates control; Epi, epicardium; Endo, endocardium; PH, pulmonary hypertension; RV, right ventricle; and Sac/Val, sacubitril/valsartan.

prevented by sac/val treatment ( $5.22 \pm 0.35$ ,  $2.66 \pm 0.47$ , and  $3.96 \pm 0.65$  mg/mm<sup>3</sup> for control, PH, and sac/val, respectively).

### Biomechanics

Biaxial testing ( $n_{\text{Control}} = 11$ ,  $n_{\text{PH}} = 12$ ,  $n_{\text{Sac/Val}} = 11$ ) demonstrated significantly increased stiffness in both longitudinal and circumferential directions as a result of PH (Figure 5A). Sac/val treatment improved RVFW biaxial biomechanical properties in both directions. Fiber-level stiffness of the combined collagen and myofiber bundles increased in PH whereas sac/val treatment resulted in decreased stiffness compared with PH levels (Figure 5B). Furthermore, the intrinsic myofiber stiffness of RV specimens increased in PH (Figure 5C, Table S4;  $168.4 \pm 101.0$  kPa for PH versus  $81.0 \pm 29.6$  kPa for control). Sac/val treatment resulted in significantly

lower stiffness than the PH cohort ( $65.4 \pm 53.4$  kPa) while showing no difference with controls. Collagen recruitment strain decreased significantly as a result of PH with sac/val demonstrating no significant effects (Figure 5D;  $10.0 \pm 2.2\%$ ,  $3.9 \pm 0.9\%$ , and  $4.4 \pm 1.2\%$  for control, PH, and sac/val, respectively).

Constitutive modeling revealed increased stiffness in the longitudinal and circumferential directions as well as increased in-plane coupling due to pulmonary artery banding (Figure 6A, Table S4; longitudinal stiffness:  $68.2 \pm 26.6$  kPa for PH versus  $16.4 \pm 5.4$  kPa for control, circumferential stiffness:  $31.5 \pm 11.3$  kPa for PH versus  $14.8 \pm 8.3$  kPa for control, coupled stiffness:  $38.3 \pm 24.9$  kPa for PH versus  $11.1 \pm 4.4$  kPa for control). Sac/val treatment resulted in significantly lower stiffness in both longitudinal and circumferential directions, but no statistically significant effects



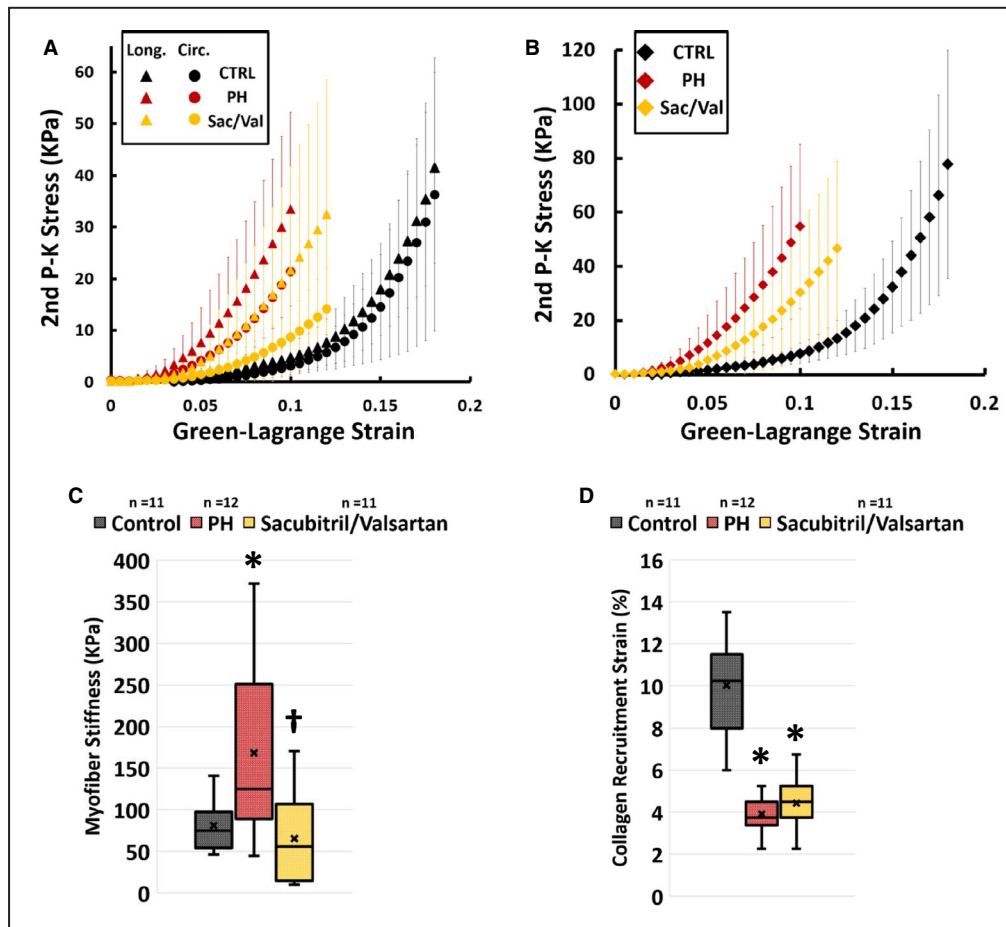


**Figure 5.** Effects of sac/val treatment on (A) biaxial mechanical properties of RVFW, (B) fiber-level mechanical properties of combined collagen and myofiber bundles, (C) intrinsic myofiber stiffness, (D) collagen recruitment strain.

Sac/val treatment resulted in improved tissue-level biomechanical properties. At the fiber level, sac/val prevented an increase in myofiber stiffness in PH but did not affect collagen recruitment strains. Horizontal line (—) and cross (x) representing median and mean of distributions, respectively. Error bars in part (A) and (B) representing SD. Kruskal–Wallis tests with pairwise Wilcoxon rank sum post hoc testing. \* $P < 0.05$  compared with control, † $P < 0.05$  compared with PH. 2<sup>nd</sup> P-K Stress indicates second Piola-Kirchhoff stress; Circ., circumferential; CTRL, control; Long., longitudinal; PH, pulmonary hypertension; RVFW, right ventricular free wall; and Sac/Val, sacubitril/valsartan.

were observed for the coupled stiffness (Figure 6A; longitudinal stiffness:  $39.1 \pm 16.9$  kPa, circumferential stiffness:  $18.7 \pm 8.4$  kPa, coupled stiffness:  $21.7 \pm 10.6$  kPa). Overall, the constitutive model used in this study showed an acceptable performance in fitting our experimental data ( $R^2$ :  $0.95 \pm 0.02$ ,  $0.91 \pm 0.05$ , and  $0.93 \pm 0.03$  for control, PH, and sac/val, respectively). Cohort-specific strain energy maps (median of strain energy distributions of samples in each cohort) demonstrate the combined effects of all model parameters on RV biomechanical properties and provide a convenient summary of the effect of PH and sac/val treatment on the biomechanics of RVFW tissue. With a certain amount of strain energy, the PH tissue deforms less than the control cohort

in both circumferential and longitudinal directions (indicating increased stiffness), whereas the sac/val strain energy map shows similar deformation patterns to controls.

## DISCUSSION

In this work, we aimed to evaluate the effectiveness sac/val treatment to prevent RV remodeling in PH. The primary findings of this study were (1) sac/val treatment decreased RV maximum pressures, improved RV contractile and relaxation functions, and prevented RV-PA uncoupling; (2) sac/val attenuated RV hypertrophy and prevented transmural reorientation of RV collagen and myofibers; and (3) sac/val resulted in

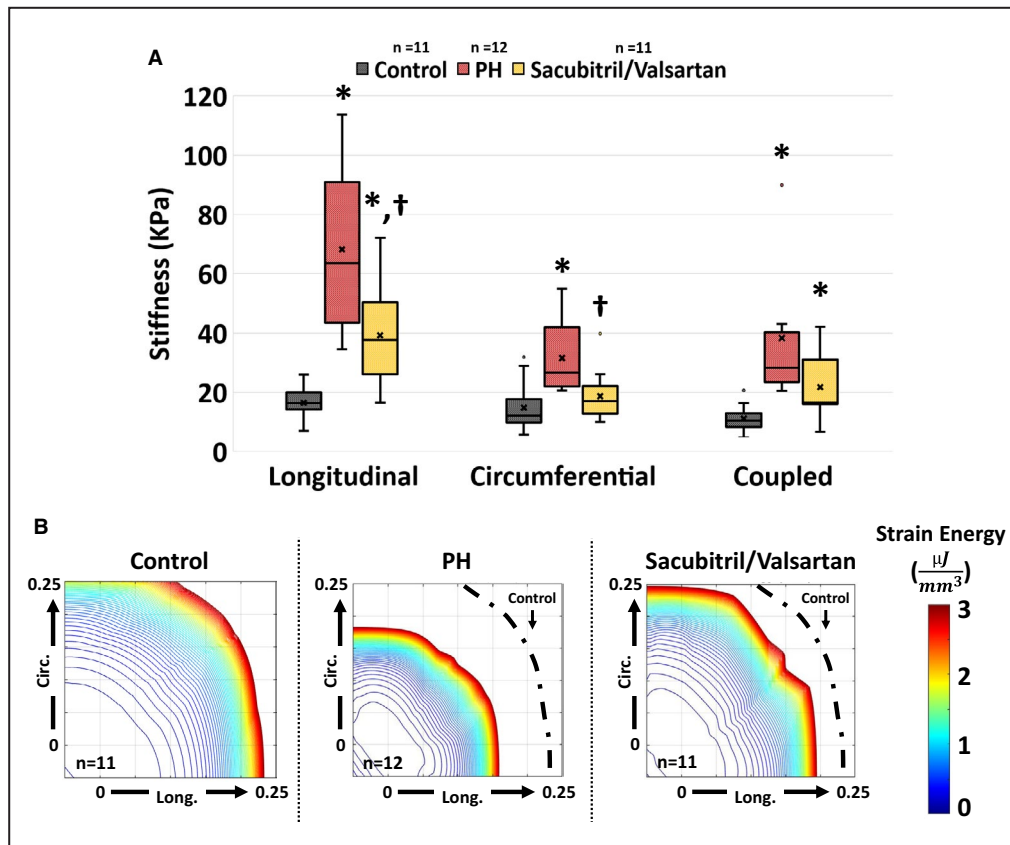


**Figure 6.** A, Longitudinal, circumferential, and coupled stiffness of RV myocardium revealed by constitutive modeling, (B) cohort-specific strain energy maps of RV myocardium, indicating increased stiffness in PH and improved biomechanical performance with sac/val treatment.

Sac/val improved RV stiffness in both circumferential and longitudinal directions with no significant effects on in-plane coupling. Dashed lines indicate the strain energy levels for the control cohort at  $3 \frac{\mu\text{J}}{\text{mm}^3}$ . Horizontal line (—) and cross (X) representing median and mean of distributions, respectively. Kruskal-Wallis tests with pairwise Wilcoxon rank sum post hoc testing. \* $P < 0.05$  compared with control, † $P < 0.05$  compared with PH. Circ. indicates circumferential; Long., longitudinal; and PH, pulmonary hypertension.

improved RV biomechanical properties at the tissue level and prevented increased myofiber stiffness in PH.

Sac/val decreased RV maximum pressures by 29% (Figure 2A). This is consistent with reported effects of sac/val in other animal models of PH.<sup>10</sup> sac/val treatment also prevented the alterations in load-dependent measures of contractility (dp/dt max) and relaxation (dp/dt min), caused by PA banding (Figure 2D and 2E; 30% reduction and 29% increase, respectively). As suggested by previous investigations,<sup>30</sup> effects of angiotensin receptor-neprilysin inhibition on load-dependent contractile and relaxation functions are likely a direct result of the synergy between sacubitril and valsartan. PA banding resulted in increased RV contractility (Ees) in response to increased afterload (Ea) (Figure 2F and 2G); however, the increased contractility was not sufficiently matched to the increased afterload, which resulted in uncoupling of RV-PA function (Ees/Ea) and decompensated RV failure (Figure 2H). Sac/val hampered an increase in RV afterload (35% improvement)

and prevented RV-PA uncoupling, while showing no significant effects on Ees (Figure 2F through 2H). Given our preventive treatment approach in this study, the observed effects on afterload more likely indicate the role of sac/val in arresting progressive RV remodeling post banding. Similar improvements in RV function, reduced PA pressures, and RV-PA recoupling were observed in recent clinical case reports on effects of sac/val treatment on 3 patients with PH due to left heart disease.<sup>31,32</sup> The observed effects in this study may suggest a direct ventricular remodeling (as opposed to pulmonary vascular remodeling) mechanism with sac/val treatment, because of the presence of a fixed arterial occlusion in our pulmonary artery banding model.

A significant increase in RV wall thickness and mass was observed in PH (Figure 3). Clinically, hypertrophy has been identified as an initial adaptive response in PH in order to increase RV contractility and the resultant chamber pressure to pump against the increased afterload.<sup>1</sup> This was also observed in our previous

studies using a similar animal model.<sup>4</sup> Similar to previous studies,<sup>10</sup> sac/val treatment resulted in significant improvements (16%) in RV hypertrophy, while not affecting RV mass, suggesting an overall increase in RVFW density with sac/val treatment compared with PH (decrease in volume with relatively similar RV mass), consistent with our histological observations of RVFW wet tissue density. In the context of improved RV function and pressures, increased tissue density may indicate a combination of decreased collagen content (fibrosis) and/or recovery of inherent collagen fiber density, although we were able to detect only a nonsignificant trend in RV fibrosis in our histological measurements.

Histological analysis revealed increased fibrosis and transmural reorientation of collagen and myofibers in PH (Figure 4A through 4C). Sac/val prevented transmural reorientation of both collagen and myofibers, showing only slight reorientations at subendocardial levels (Figure 4B and 4C). Dominant transmural orientation of myofibers (circular mean of transmural orientations) was rotated by  $\approx 15.5^\circ$  toward the longitudinal direction (apex-to-outflow tract) in PH (Figure 4D). This was also observed in other studies in a rat model of PH<sup>4,9,33</sup> and was recently hypothesized to be a mechanism underlying maladaptive RV remodeling.<sup>6</sup> Although the exact mechanism of fiber reorientation in PH remains unknown, 1 potential mechanism as suggested by others<sup>6</sup> is alterations in the biomechanical stimuli in the myofiber niche resulting from increased RV pressures, in addition to RV fiber kinematics caused by chamber dilation. A potential pathway to be investigated in future studies is the role of sac/val in preventing longitudinal fiber realignment via reduction in RV pressures, which may lead to decreased wall stress. Prevention of myofiber reorientation may be an important mechanism of action for drugs targeting the RV.

Despite demonstrating a slight reduction in RV fibrosis (13%) with sac/val treatment, this did not reach statistical significance (Figure 4E and 4F). This is interesting in light of the improved hemodynamics and RV tissue biomechanics, which may suggest that sac/val is primarily acting on RV myocytes and not on collagen or fibroblasts in this model of PH. Previous studies have demonstrated antifibrotic effects for sac/val in other animal models of PH<sup>10</sup> as well as models of LV pressure overload,<sup>16</sup> LV failure in the setting of aortic valve insufficiency,<sup>34</sup> and LV myocardial infarction.<sup>35</sup> Despite a large body of evidence in the literature indicating the antifibrotic effects of sac/val for the LV, there still exists some controversy.<sup>36,37</sup> The observed effects of sac/val treatment on RV fibrosis in this study could potentially be attributable to differences in the pathophysiology<sup>38</sup> of the RV and LV pressure overload. Further studies looking at RV-specific fibrotic responses to sac/val treatment are warranted.

PH resulted in increased RVFW tissue stiffness in both circumferential and longitudinal directions (Figure 5A), as well as increased fiber-level stiffness of combined collagen and myofiber bundles (Figure 5B). Also, the intrinsic stiffness of myofibers increased in PH (Figure 5C). This is consistent with clinical observations of reduced titin phosphorylation and increased RV cardiomyocyte sarcomere stiffness in patients with pulmonary arterial hypertension.<sup>39</sup> On the other hand, collagen recruitment strain decreased compared with controls, indicating a possible combination of increased collagen content (fibrosis) and/or alterations in the micro-architecture of collagen fibers (decrease in crimp) in PH (Figure 5D). Sac/val resulted in decreased stiffness in both longitudinal and circumferential directions as well as the fiber-level stiffness of combined myo-collagen fiber bundles (Figure 5A and 5B). The 61% reduction in intrinsic myofiber stiffness with sac/val treatment (Figure 5C) suggests a possible mechanism at the cardiomyocyte level; one such explanation to explore in future studies may be upregulation of cardiomyocyte titin phosphorylation.

Quantifying the tissue-level stiffness with constitutive modeling revealed increased stiffness in longitudinal and circumferential directions in PH (Figure 6A), accompanied by collagen and myofiber reorientation toward the longitudinal direction (increased tissue-level longitudinal stiffness out of proportion to the elevation in intrinsic myofiber stiffness). Sac/val treatment resulted in significantly lower stiffness in both directions (Figure 6A) and prevented fiber reorientation.

PH also resulted in increased in-plane coupling of longitudinal and circumferential directions with no significant benefits demonstrated by sac/val treatment (Figure 6A). Previous studies have shown that increased in-plane coupling is an indication of a more anisotropic response resulting from a more clustered fiber alignment<sup>40</sup> or increased collagen-myofiber interactions.<sup>8</sup> Histological studies of RVFW specimens (Figure 4B and 4C) showed increased range of fiber angles from epicardium to endocardium for both PH and sac/val cohorts (fiber angle range from Epi→Endo:  $60^\circ$ ,  $96^\circ$ , and  $83^\circ$  for control, PH, and sac/val, respectively). This, together with the observed increase in collagen content, explains the increased coupling stiffness in Figure 6A. The strain energy maps in Figure 6B demonstrate increased stiffness in PH (smaller deformations in both longitudinal and circumferential directions are obtained at the same strain energy levels compared with controls), whereas sac/val resulted in similar deformation patterns to controls.

Taken together, the actions of sac/val on the RV in PH seem to be a prevention of progressive and maladaptive remodeling that is linked to a prevention of myofiber reorientation, with a preferential effect on RV myocytes (as opposed to fibrosis), including prevention

of myofiber stiffening. Thus, this study provides a potential insight into the RV remodeling process in PH, in which progressive pressure overload and increasing wall stress result in alterations of the myocyte contractile apparatus. This, in turn, may lead to progressive myofiber stiffening and fiber angle reorientation, all of which contributes to RV-PA uncoupling and RV failure. Drugs that can have a direct effect on this potential remodeling process of the myocyte contractile apparatus, as sac/val may,<sup>41,42</sup> should be further studied in PH and may provide a unique and highly beneficial therapeutic option.

There are limitations to the experimental and modeling techniques used in this study. The PA banding model of PH results in a myocyte hypertrophy-dominated response as opposed to extracellular matrix remodeling and fibrosis.<sup>4</sup> This model helps us to focus on the RV myocardium in the absence of confounding conditions such as hypoxia or pulmonary circulation disease, as we aimed to study the effects of sac/val specifically on RV biomechanics. Other animal models of PH<sup>10,18</sup> might be better suited for studying the fibrotic response of the RV. Moreover, we employed a preventive treatment approach to analyze the effects of sac/val on PH in a 3-week period. However, this may not precisely mimic what is observed with regard to clinical presentation of PH in humans. Different treatment windows as well as treatment scenarios after fully developing PH needs to be further investigated. An isolated angiotensin receptor blocking cohort (valsartan-only treatment) was not included in the current work, mainly because of the evidence from previous studies<sup>10,43,44</sup> demonstrating no significant hemodynamic or RV hypertrophy benefits with isolated use of angiotensin II receptor antagonists in PH (which limits the translation of any potential biomechanical benefits from Valsartan-only treatment). Nevertheless, this limits our findings to the effects of combination therapy with sac/val (the synergistic effects of angiotensin receptor-neprilysin inhibition) without looking at independent benefits from Valsartan or Sacubitril alone. We also did not include a known pure vasodilator with limited direct cardiac effects, which might provide evidence of a differential effect of sac/val; however, the pulmonary artery banding model was felt to not be suitable to this approach. Paraffin fixation processes for histological analysis may cause artifacts in fiber coherency analysis caused by tissue dehydration and shrinkage; however, this will affect all groups studied equally allowing for adequate comparison between groups. Also, here we used a phenomenological constitutive model to analyze the tissue-level biomechanics of RV myocardium. Future studies will employ a structurally detailed constitutive model (such as in Avazmohammadi et al<sup>8</sup>) to study the effects of transmural fiber architectures and interactions between collagen and myofibers in more detail.

## CONCLUSIONS

Sac/val may prevent maladaptive RV remodeling in a pressure overload model via amelioration of RV pressure rise, hypertrophy, collagen and myofiber reorientation as well as tissue stiffening both at the tissue and myofiber level. Further study of the role of sac/val treatment in PH and RV remodeling is warranted.

## ARTICLE INFORMATION

Received December 20, 2019; accepted April 24, 2020.

### Affiliations

From the Departments of Bioengineering (D.S.K., T.N.B., C.T., K.K., M.A.S.) and Mechanical Engineering and Materials Science (K.K.), Division of Cardiology, School of Medicine (K.K., M.A.S.), McGowan Institute for Regenerative Medicine (K.K., M.A.S.), and Center for Ultrasound Molecular Imaging and Therapeutics (K.K.), University of Pittsburgh, PA; Heart and Vascular Institute, University of Pittsburgh Medical Center (UPMC), Pittsburgh, PA (E.B., K.K., M.A.S.); Pittsburgh Heart, Lung, Blood and Vascular Medicine Institute, University of Pittsburgh and University of Pittsburgh Medical Center (UPMC), Pittsburgh, PA (T.N.B., K.K., M.A.S.).

### Acknowledgments

The authors would like to acknowledge Gemin Ni, MD for performing the pulmonary artery banding procedures in this study.

### Sources of Funding

This study was supported by an Investigator Initiated Grant from Novartis Pharmaceutical Corporation to Dr Simon. Dr Simon is also supported by the NIH grants 1R01AG058659, 2P01HL103455, UL1 TR001857. Sharifi Kia is supported by a fellowship grant from the American Heart Association (AHA Award No. 20PRE35210429).

### Disclosures

Simon reports research support from Novartis, Aadi and consultancy fees from Complexa, Actelion, and United Therapeutics. The remaining authors have no disclosures to report.

### Supplementary Materials

Tables S1–S4

## REFERENCES

- Voelke NF, Natarajan R, Drake JI, Bogaard HJ. Right ventricle in pulmonary hypertension. *Compr Physiol*. 2011;1:525–540.
- Benza RL, Park MH, Keogh A, Girgis RE. Management of pulmonary arterial hypertension with a focus on combination therapies. *J Heart Lung Transplant*. 2007;26:437–446.
- Humbert M, Sitbon O, Yaïci A, Montani D, O’Callaghan DS, Jaïs X, Parent F, Savane L, Natali D, Günther S, et al. Survival in incident and prevalent cohorts of patients with pulmonary arterial hypertension. *Eur Respir J*. 2010;36:549–555.
- Hill MR, Simon MA, Valdez-Jasso D, Zhang W, Champion HC, Sacks MS. Structural and mechanical adaptations of right ventricle free wall myocardium to pressure overload. *Ann Biomed Eng*. 2014;42:2451–2465.
- Jang S, Vanderpool RR, Avazmohammadi R, Lapshin E, Bachman TN, Sacks M, Simon MA. Biomechanical and hemodynamic measures of right ventricular diastolic function: translating tissue biomechanics to clinical relevance. *J Am Heart Assoc*. 2017;6:e006084. DOI: 10.1161/JAHA.117.006084.
- Avazmohammadi R, Mendiola EA, Li DS, Vanderslice P, Dixon RAF, Sacks MS. Interactions between structural remodeling and hypertrophy in the right ventricle in response to pulmonary arterial hypertension. *J Biomech Eng*. 2019;141:910161–13.
- Carruth ED, McCulloch AD, Omens JH. Transmural gradients of myocardial structure and mechanics: implications for fiber stress and strain in pressure overload. *Prog Biophys Mol Biol*. 2016;122:215–226.



8. Avazmohammadi R, Hill MR, Simon MA, Zhang W, Sacks MS. A novel constitutive model for passive right ventricular myocardium: evidence for myofiber-collagen fiber mechanical coupling. *Biomech Model Mechanobiol.* 2017;16:561–581.
9. Avazmohammadi R, Hill M, Simon M, Sacks M. Transmural remodeling of right ventricular myocardium in response to pulmonary arterial hypertension. *APL Bioeng.* 2017;1:16105.
10. Clements RT, Vang A, Fernandez-Nicolas A, Kue NR, Mancini TJ, Morrison AR, Mallem K, McCullough DJ, Choudhary G. Treatment of pulmonary hypertension with angiotensin II receptor blocker and neprilysin inhibitor sacubitril/valsartan. *Circ Heart Fail.* 2019;12:e005819.
11. Menendez JT. The mechanism of action of LCZ696. *Card Fail Rev.* 2016;2:40.
12. McMurray JJV, Packer M, Desai AS, Gong J, Lefkowitz MP, Rizkala AR, Rouleau JL, Shi VC, Solomon SD, Swedberg K, et al. Angiotensin-neprilysin inhibition versus enalapril in heart failure. *N Engl J Med.* 2014;371:993–1004.
13. Gu J, Noe A, Chandra P, Al-Fayoumi S, Ligueros-Saylan M, Sarangapani R, Maahs S, Ksander G, Rigel DF, Jeng AY, et al. Pharmacokinetics and pharmacodynamics of LCZ696, a novel dual-acting angiotensin receptor-neprilysin inhibitor (ARNi). *J Clin Pharmacol.* 2010;50:401–414.
14. Pu Q, Brassard P, Javeshghani DM, Iglarz M, Webb RL, Amiri F, Schiffrin EL. Effects of combined AT1receptor antagonist/NEP inhibitor on vascular remodeling and cardiac fibrosis in SHRSP. *J Hypertens.* 2008;26:322–333.
15. Von Lueder TG, Sangaralingham SJ, Wang BH, Kompa AR, Atar D, Burnett JC, Krum H. Renin-angiotensin blockade combined with natriuretic peptide system augmentation novel therapeutic concepts to combat heart failure. *Circ Heart Fail.* 2013;6:594–605.
16. Burke RM, Lighthouse JK, Mickelsen DM, Small EM. Sacubitril/valsartan decreases cardiac fibrosis in left ventricle pressure overload by restoring PKG signaling in cardiac fibroblasts. *Circ Heart Fail.* 2019;12:e005565.
17. Valdez-Jasso D, Simon MA, Champion HC, Sacks MS. A murine experimental model for the mechanical behaviour of viable right-ventricular myocardium. *J Physiol.* 2012;590:4571–4584.
18. Bogaard HJ, Natarajan R, Henderson SC, Long CS, Kraskauskas D, Smithson L, Ockaili R, McCord JM, Voelkel NF. Chronic pulmonary artery pressure elevation is insufficient to explain right heart failure. *Circulation.* 2009;120:1951–1960.
19. Faber MJ, Dalinghaus M, Lankhuizen IM, Steendijk P, Hop WC, Schoemaker RG, Duncker DJ, Lamers JMJ, Helbing WA. Right and left ventricular function after chronic pulmonary artery banding in rats assessed with biventricular pressure-volume loops. *Am J Physiol Heart Circ Physiol.* 2006;291:H1580–H1586.
20. Rezakhanliha R, Agianniotis A, Schrauwen JTC, Griffa A, Sage D, Bouten CVC, Van De Vosse FN, Unser M, Stergiopoulos N. Experimental investigation of collagen waviness and orientation in the arterial adventitia using confocal laser scanning microscopy. *Biomech Model Mechanobiol.* 2012;11:461–473.
21. Püspöki Z, Storath M, Sage D, Unser M. Transforms and operators for directional bioimage analysis: a survey. *Adv Anat Embryol Cell Biol.* 2016;219:69–93.
22. Sacks MS. A method for planar biaxial mechanical testing that includes in-plane shear. *J Biomech Eng.* 1999;121:551–555.
23. Zhang W, Feng Y, Lee C-H, Billiar KL, Sacks MS. A generalized method for the analysis of planar biaxial mechanical data using tethered testing configurations. *J Biomech Eng.* 2015;137:64501–64513.
24. Fata B, Zhang W, Amini R, Sacks MS. Insights into regional adaptations in the growing pulmonary artery using a meso-scale structural model: effects of ascending aorta impingement. *J Biomech Eng.* 2014;136:021009.
25. Humphrey JD, Rajagopal KR. A constrained mixture model for growth and remodeling of soft tissues. *Math Models Methods Appl Sci.* 2002;12:407–430.
26. Choi HS, Vito RP. Two-dimensional stress-strain relationship for canine pericardium. *J Biomech Eng.* 1990;112:153–159.
27. Kural MH, Cai M, Tang D, Gwyther T, Zheng J, Billiar KL. Planar biaxial characterization of diseased human coronary and carotid arteries for computational modeling. *J Biomech.* 2012;45:790–798.
28. Berens P. CircStat: a MATLAB toolbox for circular statistics. *J Stat Softw.* 2009;31:1–21.
29. R Core Team. *R: A Language and Environment for Statistical Computing.* Vienna, Austria: R Foundation for Statistical Computing; 2018.
30. Maslov MY, Foianini S, Mayer D, Orlov MV, Lovich MA. Synergy between sacubitril and valsartan leads to hemodynamic, antifibrotic, and exercise tolerance benefits in rats with preexisting heart failure. *Am J Physiol Heart Circ Physiol.* 2019;316:H289–H297.
31. De Simone V, Guarise P, Zanotto G, Morando G. Reduction in pulmonary artery pressures with use of sacubitril/valsartan. *J Cardiol Cases.* 2019;20:187–190.
32. Giammarresi A, Bandera F, Losito M, Labate V, Alfonzetti E, Guazzi M. Effect of sacubitril/valsartan on pulmonary hypertension due to left heart disease. *Eur Heart J Cardiovasc Imaging.* 2019;20:i1197.
33. Avazmohammadi R, Mendiola EA, Soares JS, Li DS, Chen Z, Merchant S, Hsu EW, Vanderslice P, Dixon RAF, Sacks MS. A computational cardiac model for the adaptation to pulmonary arterial hypertension in the rat. *Ann Biomed Eng.* 2019;47:138–153.
34. Maslov MY, Foianini S, Mayer D, Orlov MV, Lovich MA. Interaction between sacubitril and valsartan in preventing heart failure induced by aortic valve insufficiency in rats. *J Card Fail.* 2019;25:921–931.
35. Pfau D, Thorn SL, Zhang J, Mikush N, Renaud JM, Klein R, DeKemp RA, Wu X, Hu X, Sinusas AJ, et al. Angiotensin receptor neprilysin inhibitor attenuates myocardial remodeling and improves infarct perfusion in experimental heart failure. *Sci Rep.* 2019;9:5791.
36. Zannad F, Ferreira JP. Is sacubitril/valsartan antifibrotic? *J Am Coll Cardiol.* 2019;73:807–809.
37. Zile MR, O'Meara E, Claggett B, Prescott MF, Solomon SD, Swedberg K, Packer M, McMurray JJV, Shi V, Lefkowitz M, et al. Effects of sacubitril/valsartan on biomarkers of extracellular matrix regulation in patients with HFrEF. *J Am Coll Cardiol.* 2019;73:795–806.
38. Frangogiannis NG. Fibroblasts and the extracellular matrix in right ventricular disease. *Cardiovasc Res.* 2017;113:1453–1464.
39. Rain S, Handoko ML, Trip P, Gan CTJ, Westerhof N, Stienen GJ, Paulus WJ, Ottenheim CAC, Marcus JT, Dorfmueller P, et al. Right ventricular diastolic impairment in patients with pulmonary arterial hypertension. *Circulation.* 2013;128:2016–2025.
40. Billiar KL, Sacks MS. Biaxial mechanical properties of the native and glutaraldehyde-treated aortic valve cusp: part II—a structural constitutive model. *J Biomech Eng.* 2000;122:327–336.
41. Trivedi RK, Polhemus DJ, Li Z, Yoo D, Koiwaya H, Scarborough A, Goodchild TT, Lefer DJ. Combined angiotensin receptor-neprilysin inhibitors improve cardiac and vascular function via increased NO bioavailability in heart failure. *J Am Heart Assoc.* 2018;7:e008268. DOI: 10.1161/JAHA.117.008268.
42. Iborra-Egea O, Gálvez-Montón C, Roura S, Perea-Gil I, Prat-Vidal C, Soler-Botija C, Bayes-Genis A. Mechanisms of action of sacubitril/valsartan on cardiac remodeling: a systems biology approach. *NPJ Syst Biol Appl.* 2017;3:12.
43. Borgdorff MA, Bartelds B, Dickinson MG, Steendijk P, Berger RMF. A cornerstone of heart failure treatment is not effective in experimental right ventricular failure. *Int J Cardiol.* 2013;169:183–189.
44. Andersen S, Schultz JG, Andersen A, Ringgaard S, Nielsen JM, Holmboe S, Vildbrad MD, De Man FS, Bogaard HJ, Vonk-Noordegraaf A, et al. Effects of bisoprolol and losartan treatment in the hypertrophic and failing right heart. *J Card Fail.* 2014;20:864–873.

# **SUPPLEMENTAL MATERIAL**

**Table S1. p values obtained for pairwise comparison of different hemodynamic outcomes.**

	<b>Control vs. PH</b>	<b>Control vs. Sac/Val</b>	<b>PH vs. Sac/Val</b>
<b>Maximum Pressure (<math>P_{\max}</math>)</b>	<0.0001	<0.0001	0.0018
<b>Stroke Volume</b>	0.0033	0.1113	1.0
<b>dP/dt<sub>max</sub></b>	<0.0001	0.0015	0.0119
<b>dP/dt<sub>min</sub></b>	<0.0001	0.0004	0.0426
<b>PA Elastance (<math>E_a</math>)</b>	<0.0001	0.0002	0.0158
<b>RV Elastance (<math>E_{es}</math>)</b>	<0.0001	0.0110	0.8440
<b><math>E_{es}/E_a</math></b>	0.0005	0.5914	0.1087

**Table S2. p values obtained for pairwise comparison of morphological measurements.**

	<b>Control vs. PH</b>	<b>Control vs. Sac/Val</b>	<b>PH vs. Sac/Val</b>
<b>RVFW Thickness</b>	<0.0001	<0.0001	0.0061
<b>RV/LV Mass Ratio</b>	<0.0001	<0.0001	0.5500

**Table S3. p values obtained for pairwise comparison of histological measurements.**

	<b>Control vs. PH</b>	<b>Control vs. Sac/Val</b>	<b>PH vs. Sac/Val</b>
<b>Dominant Myofiber Direction</b>	0.0026	0.5687	0.0106
<b>Collagen Area Fraction</b>	0.0444	0.0065	1.0
<b>RVFW Density</b>	0.0049	0.1246	0.1487

**Table S4.** p values obtained for pairwise comparison of biaxial mechanical properties and constitutive modeling results.

	<b>Control vs. PH</b>	<b>Control vs. Sac/Val</b>	<b>PH vs. Sac/Val</b>
<b>Myofiber Stiffness</b>	0.0470	1.0	0.0320
<b>Collagen Recruitment Strain</b>	0.0002	0.0003	0.7023
<b>Long. Stiffness (<math>B_0*b_1</math>)</b>	<0.0001	0.0003	0.0259
<b>Circ. Stiffness (<math>B_0*b_2</math>)</b>	0.0022	0.3990	0.0039
<b>Coupled Stiffness (<math>B_0*b_3</math>)</b>	<0.0001	0.0160	0.0950